*Inorg. Chem.* **2005**, *44*, 7099–7108


# Tuning of Spin Transition in Radical-Containing Iron(III) Complexes by Remote Ligand Substituents

**Soumen Mukherjee, Thomas Weyhermüller, Eckhard Bill, Karl Wieghardt, and Phalguni Chaudhuri***

*Max-Planck-Institute for Bioinorganic Chemistry, Stiftstrasse 34-36, D-45470 Mülheim an der Ruhr, Germany*

Received June 2, 2005

Two new iron(III) complexes, $Fe^{III}(L^{F\bullet})_3$ (**1**) and $Fe^{III}(L^{t-Bu\bullet})_3$ (**2**), of remote substituted *o*-aminophenol-based ligands are reported; complexes **1** and **2** contain three O,N-coordinated *o*-iminobenzosemiquinonate(1–) radical anions with ferric centers in high-spin and low-spin configurations. The crystal structures of **1** and **2** were determined by X-ray diffraction at 100 and 293 K, and the electronic structures were established by various physical methods including Mössbauer (4–290 K) and variable-temperature (2–290 K) susceptibility measurements. Electrochemical measurements (cyclic and square-wave voltammetry) indicate primarily ligand-centered redox processes. Complex **1**, with the more electron-withdrawing fluoro substituents, retains the high-spin character of the ferric ion throughout the temperature range studied (2–290 K) and exhibits, as expected, strong antiferromagnetic coupling operating between three radicals ($S_R = 1/2$) and the high-spin Fe(III) center ($S_{Fe} = 5/2$) yielding an $S_t = 1$ as the ground state. In contrast, the occurrence of a thermally induced spin crossover process ($S_{Fe} = 5/2 \leftrightarrow S_{Fe} = 1/2$) is observed for complex **2** $Fe^{III}(L^{t-Bu\bullet})_3$, in which more electron donating *tert*-butyl substituents in the ligand are present. A rationale for the control of the electronic state of ferric ions in **2** together with spin-coupling schemes for **1** and **2** are provided.

## Introduction

The spin-transition phenomenon (LS ↔ HS) appears to remain one of the fascinating examples of transitions between two electronic states in molecular chemistry since the pioneering work of Cambi and co-workers[1] in the 1930s on the unusual temperature-dependent magnetism of iron(III) complexes of various dithiocarbamates. In the past 70 years, a significant number of Fe(III) complexes with a wide range of donor atoms, Se, S, O, and N, has been reported to exhibit a high-spin−low-spin transition, although the largest number of such examples is found for Fe(II) complexes with $d^6$ electron configuration due to reasons lying in the ligand field theory.[2] This surge of interest in general for the spin crossover phenomenon is the growing awareness that this phenomenon has potential application in molecular electronics involving switching, sensing, memory, and other devices, thus making this field relevant to many different areas, ranging from chemistry to solid-state physics and even to biology.

Moreover, redox-active paramagnetic ligands are gaining increasing interest due to their promising role in molecular magnetism.[3,4] Redox-active molecules are uniquely suited for correlating exchange coupling in polyradical oxidation states with spin/charge delocalization in mixed-valent oxidation states. We have shown in a series of papers[5] that 2-aminophenolate can coordinate to transition metal ions in

* To whom correspondence should be addressed. E-mail: Chaudh@mpi-muelheim.mpg.de.

(1) (a) Cambi, L.; Szegö, L. *Ber.* **1931**, *64*, 2591−2598. (b) Cambi, L.; Szegö, L. *Ber.* **1933**, *66*, 656−661. (c) Cambi, L.; Malatesta, L. *Ber.* **1937**, *70*, 2067−2078.

(2) *Spin Crossover in Transition Metal Compounds*; Gütlich, P., Goodwin, H. A., Eds.; Springer-Verlag: Berlin, 2004.

(3) (a) Caneschi, A.; Gatteschi, D.; Rey, P. *Prog. Inorg. Chem.* **1992**, *39*, 331−429. (b) Pierpont, C. G.; Lange, C. W. *Prog. Inorg. Chem.* **1994**, *41*, 331−442. (c) Kaim, W. *Dalton Trans.* **2003**, 761−768.

(4) Pierpont, C. G. *Coord. Chem. Rev.* **2001**, 216−217, 99−125 and **2001**, 219−221, 415−433.

(5) (a) Verani, C. N.; Gallert, S.; Bill, E.; Weyhermüller, T.; Wieghardt, K.; Chaudhuri, P. *Chem. Commun.* **1999**, 1747−1748. (b) Chaudhuri, P.; Verani, C. N.; Bill, E.; Bothe, E.; Weyhermüller, T.; Wieghardt, K. *J. Am. Chem. Soc.* **2001**, *123*, 2213−2223. (c) Chun, H.; Verani, C. N.; Chaudhuri, P.; Bothe, E.; Bill, E.; Weyhermüller, T.; Wieghardt, K. *Inorg. Chem.* **2001**, *40*, 4157−4166. (d) Kokatam, S.; Weyhermüller, T.; Bothe, E.; Chaudhuri, P.; Wieghardt, K. *Inorg. Chem.* **2005**, in press. (e) Mukherjee, S.; Weyhermüller, T.; Wieghardt, K.; Chaudhuri, P. *Dalton Trans.* **2003**, 3483−3485. (f) Mukherjee, S.; Weyhermüller, T.; Bothe, E.; Wieghardt, K.; Chaudhuri, P. *Dalton Trans.* **2004**, 3842−3853 and references therein.

10.1021/ic050885l CCC: $30.25 
Published on Web 08/27/2005

the presence of air in their oxidized paramagnetic *o*-iminobenzosemiquinone radical form $[L^{\bullet}]^{1-}$ as depicted below.

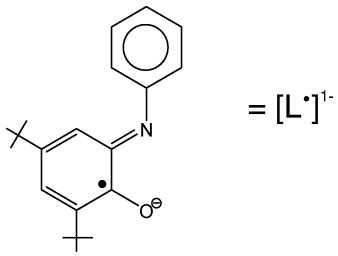


We have reported that the octahedral complex $[Fe^{III}(L^{\bullet})_3]$ possesses an $S_t = 1$ ground state where a high-spin ferric ion ($S_{Fe} = 5/2$) is intramolecularly antiferromagnetically coupled to three radical anions $[L^{\bullet}]^{1-}$ ($S_R = 1/2$). It is known that the introduction of substituents into the benzene ring of a ligand alters the ligand field strength, since the transfer of the polar properties of the substituent through the benzene ring is facilitated by the $\pi$-delocalization in the ring. Hence, we have extended our previous study on ferric complexes in this work to different substituted aniline ligands to scrutinize the effect of ring substituents on the ligating property of $H_2L^R$ in comparison to that of unsubstituted $H_2L^H$ described earlier by us.[5c] The complexes and the ligands used are shown in Scheme 1.

Here we report the syntheses, the electronic structures, and molecular structures of complexes **1** and **2**, which contain three O,N-coordinated *o*-iminobenzosemiquinonate(1−) radical anions with ferric centers in high-spin and low-spin configurations, respectively. No bidentate N,O-chelating donor set is known to impart spin-transition property until now in any ferric complex.[6]

## Experimental Section

**Materials and Physical Measurements.** Reagent- or analytical-grade materials were obtained from commercial suppliers and used without further purification, except those for electrochemical measurements. Elemental analyses (C, H, N, and Fe) were performed by the Microanalytical Laboratory, Mülheim, Germany. Fourier transform IR spectra of the samples in KBr disks were recorded with a Perkin-Elmer 2000 FT-IR instrument. Electronic absorption spectra in solution were measured with a Perkin-Elmer Lambda 19 spectrophotometer. Cyclic voltammetric and coulometric measurements were performed using EG&G equipment (potentiostat/galvanostat model 273A). Mass spectra were recorded with either a Finnigan MAT 8200 (electron ionization, EIMS) or a MAT95 (electrospray, ESI-MS) instrument. A Bruker DRX 400 instrument was used for NMR spectroscopy. Magnetic susceptibilities of powdered samples were recorded with a SQUID magnetometer in the temperature range 2−295 K with an applied field of 1 T. Experimental susceptibility data were corrected for the underlying diamagnetism using Pascal's constants and for the TIP contributions.

Mössbauer data were recorded on alternating constant-acceleration spectrometers. The sample temperature was maintained constant in an Oxford Variox- or a Mössbauer-spectromag cryostat. The latter is a split-pair superconducting magnet system for applying fields up to 8 T to the samples that can be kept at temperatures in the range 1.5−250 K. The field at the sample is perpendicular to the $\gamma$-beam. With the help of re-entrant bore tubes, the $^{57}$Co/Rh source was positioned at room-temperature inside the gap of the magnet system at a distance of about 85 mm from the sample. The field is zero at this position. Isomer shifts are given relative to α-Fe at room temperature.

**Scheme 1**

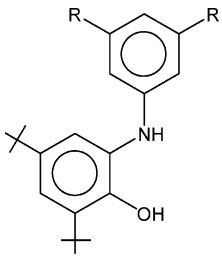


R = -F, $H_2L^F$
R = -C(CH$_3$)$_3$, $H_2L^{t\text{-}Bu}$
R = -H, $H_2L^H$

$Fe(L^{F\bullet})$ Complex **1**
$Fe(L^{t\text{-}Bu\bullet})_3$ Complex **2**
$Fe(L^{H\bullet})_3$ Complex **3**

**X-ray Crystallographic Data Collection and Refinement of the Structures.** The crystallographic data for **1** and **2** are summarized in Table 1. Graphite-monochromated Mo Kα radiation ($\lambda$ = 0.71073 Å) was used. Dark green crystals of **1** and **2** were fixed with perfluoropolyether onto glass fibers and mounted on a Nonius-Kappa CCD diffractometer equipped with a cryogenic nitrogen cold stream, and intensity data were collected at 100(2) K for **1** and **2**. Intensity data for **2** were also collected at room temperature 293 K. Final cell constants were obtained from a least-squares fit of the setting angles of all integrated reflections. Intensity data were corrected for Lorentz and polarization effects. The data sets were corrected for absorption using the Gaussian-type absorption correction routine embedded in XPREP. The Siemens ShelXTL software package[7a] was used for solution refinement[7b] and artwork of the structures; the neutral atom scattering factors of the program were used.

**Preparation of Ligands $H_2L^{t-Bu}$ and $H_2L^F$.** The ligands were prepared according to a very similar procedure described in ref 5f.

MP, IR, $^1$H NMR, $^{13}$C NMR, EI-MS, and microanalytical data for $H_2L^{t-Bu}$ have been reported earlier.[5f]

**$H_2L^F$.** Mp: 154 °C. IR (KBr, cm$^{-1}$): 3440s, 3363s, 3350s, 3113w, 2962s, 1628s, 1598s, 1478s, 1311m, 1227m, 1114s, 1000s, 830s, 667m. $^1$H NMR ($CDCl_3$): $\delta$ 1.26(s, 9H), 1.42(s, 9H), 5.15-(s, 1H), 6.10−6.16(m, 3H), 6.26(m, 1H), 6.97−6.98(d, 1H), 7.24-(s, 1H). $^{13}$C NMR ($CDCl_3$): $\delta$ 29.47, 31.51, 34.35, 35.01, 94.93, 95.35, 97.66, 97.94, 98.11, 121.63, 122.90, 126.08, 135.87, 142.66, 149.13, 149.47. $^{13}$C NMR ($CH_3OH$): $\delta$ 30.11, 32.02, 35.16, 36.03, 93.48, 97.67, 98.12, 122.31, 122.46, 128.97, 137.62, 143.15. EI-MS: *m*/*z* (relative intensity %) 334(22), 333(100), 319(18), 318-(85), 262(10), 57(46), 41(11). Calcd fw = 333.42 g/mol. Anal. Calcd for $C_{20}H_{25}F_2NO$: C, 72.05; H, 7.56; N, 4.20. Found: C, 70.3; H, 7.6; N, 4.3. The purity of the ligand was determined to be 99.3% by gas chromatographic analysis.

**Preparation of Complexes.** Complexes **1** $[Fe(L^{F\bullet})_3]$ and **2** $[Fe(L^{t-Bu\bullet})_3]$ were prepared by a similar protocol. To a degassed solution of $CH_3OH$ (20 mL) containing the ligand (1 mmol), Fe-$(ClO_4)_2 \cdot 6H_2O$ (0.25 mmol) was added. Upon addition of $NEt_3$ (0.4 mL), the color of the solution turned deep green. The solution was refluxed in air for 1 h and filtered to remove any solid particles. The deep green microcrystalline solid separated after cooling was

(6) van Koningsbruggen, P. J.; Maeda, Y.; Oshio, H. *Top. Curr. Chem.* **2004**, *233*, 259−324.

(7) (a) Sheldrick, G. M. SHELXTL Ver. 5. Siemens Analytical X-ray Instruments, Inc.: , 1994. (b) Sheldrick, G. M. SHELXL-97; University of Göttingen: Göttingen, Germany, 1997.

**Table 1.** Crystallographic Data for $Fe^{III}(L^F)_3$ (**1**) and $Fe^{III}(L^{t-Bu})_3$ (**2**) at 100(2) and 293(2) K

| | complex **2** | complex **2** | complex **1** |
|---|---|---|---|
| empirical formula | $C_{84}H_{123}FeN_3O_3$ | $C_{84}H_{123}FeN_3O_3$ | $C_{60}H_{69}F_6FeN_3O_3$ |
| fw | 1278.70 | 1278.70 | 1050.03 |
| temperature | 100(2) K | 293(2) K | 100(2) K |
| wavelength | 0.71073 Å | 0.71073 Å | 0.71073 Å |
| cryst syst, space group | monoclinic, $P2_1/c$ | monoclinic, $P2_1/c$ | monoclinic, $C2/c$ |
| unit cell dimension | $a = 16.656(2)$ Å $\alpha = 90°$<br>$b = 14.648(2)$ Å $\beta = 97.32(1)°$<br>$c = 33.433(3)$ Å $\gamma = 90°$ | $a = 17.0012(8)$Å $\alpha = 90°$<br>$b = 14.8159(6)$ Å $\beta = 96.76(1)°$<br>$c = 33.897(2)$ Å $\gamma = 90°$ | $a = 25.6710(4)$ Å $\alpha = 90°$<br>$b = 24.8786(4)$ Å $\beta = 105.50(1)°$<br>$c = 17.9867(3)$ Å $\gamma = 90°$ |
| volume (Å$^3$), $Z$ | 8090.4(16), 4 | 8478.9(7), 4 | 11069.6(3), 8 |
| density (calcd), mg/m$^3$ | 1.050 | 11.002 | 1.260 |
| abs coeff, mm$^{-1}$ | 0.232 | 0.221 | 0.339 |
| $F(000)$ | 2792 | 2792 | 4432 |
| cryst size, mm | 0.32 × 0.11 × 0.08 | 0.32 × 0.11 × 0.08 | 0.27 × 0.19 × 0.18 |
| abs correction | Gaussian, face-indexed | Gaussian, face-indexed | Gaussian, face-indexed |
| refinement method | full-matrix least-squares on $F^2$ | full-matrix least-squares on $F^2$ | full-matrix least-squares on $F^2$ |
| data/restraints/params | 20 013/0/820 | 12 467/216/893 | 17 667/39/700 |
| GOF on $F^2$ | 1.037 | 1.023 | 1.038 |
| final R indices [$I > 2\sigma(I)$] | R1 = 0.0485, wR2 = 1.1093 | R1 = 0.0688, wR2 = 0.1563 | R1 = 0.0384, wR2 = 0.0946 |
| R indices (all data) | R1 = 0.0690, wR2 = 0.1195 | R1 = 0.1024, wR2 = 0.1748 | R1 = 0.0458, wR2 = 0.0989 |
| largest diff. peak and hole | 1.009 and −0.459 e·A$^{-3}$ | 0.333 and −0.285 e·A$^{-3}$ | 0.635 and −0.370 e·A$^{-3}$ |

recrystallized from $CH_2Cl_2$−$CH_3CN$ (1:1) for **1** and from $Et_2O$−$CH_3CN$ for **2**.

**Complex 1.** Yield: 0.16 g (63%). Anal. Calcd for $C_{60}H_{69}F_6FeN_3O_3$ (fw = 1050.07 g/mol): C, 68.63; H, 6.62; N, 4.0; Fe, 5.32. Found: C, 68.5; H, 6.7; N, 4.0; Fe, 5.3. IR (KBr, cm$^{-1}$): 2960s, 2909m, 2871m, 1612s, 1591s, 1468s, 1428s, 1248m, 1134s, 1116s, 990s. UV−vis ($CH_2Cl_2$) [$\lambda_{max}$/nm, $\epsilon$/M$^{-1}$ cm$^{-1}$)]: 745 (9.26 × 10$^3$), 435sh (∼7.0 × 10$^3$), 302 (1.785 × 10$^4$). MS(EI): 1049 [M$^+$, 21%], 718 [(M − L)$^+$, 100%].

**Complex 2.** Yield: 0.22 g (69%). Anal. Calcd for $C_{84}H_{123}FeN_3O_3$ (fw = 1218.70 g/mol): C, 78.95; H, 9.70; N, 3.29; Fe, 4.37. Found: C, 77.9; H, 9.2; N, 3.2; Fe, 4.6. IR (KBr, cm$^{-1}$): 2957s, 2905m, 2868m, 1581m, 1468m, 1362m, 1247m, 1003m, 945m. UV−vis ($CH_2Cl_2$) [$\lambda_{max}$/nm, $\epsilon$/M$^{-1}$ cm$^{-1}$)]: 750 (9.22 × 10$^3$), 441sh (∼6.57 × 10$^3$), 302 (3.28 × 10$^4$). MS(EI): 1278 [M$^+$, 27%], 870 [(M − L)$^+$, 100%].

## Results and Discussion

Preparations of mononuclear iron complexes containing three O,N-coordinated, bidentate ligands have been performed in a straightforward fashion in methanol by the reaction of $[Fe(OH_2)_6]ClO_4$, the ligand, and a suitable base like $NEt_3$ in the presence of air at elevated temperatures. A deep green microcrystalline solid was obtained in moderate yield, and repeated recrystallization resulted in X-ray quality crystals. Complexes **1**, $Fe(L^{F\bullet})_3$, and **2**, $Fe(L^{t-Bu\bullet})_3$, were analyzed by elemental analysis and various spectroscopic techniques, viz., IR, UV−vis, and MS in EI-mode.

The most salient features observed for **1** and **2** in the IR are the absence of the frequencies attributable to $\nu$(NH) and $\nu$(OH) stretching and the appearance of the $\nu$(C═N) band at 1581 cm$^{-1}$ for **2**, whereas this band is split into two sharp bands at 1612 and 1591 cm$^{-1}$ for **1**. A sharp peak at ∼1450 cm$^{-1}$ due to $\nu$(C−O) appear for both complexes. Mass spectroscopy for the complexes exhibits molecular peak in the EI mode. Details of the IR peaks and mass spectrometric data are summarized in the Experimental Section.

The electronic spectra of **1** and **2** in dichloromethane solution at room temperature exhibit maxima: 745 ($\epsilon$ = 9260 M$^{-1}$ cm$^{-1}$) and 435 nm ($\epsilon \approx$ 7000 M$^{-1}$ cm$^{-1}$) for **1** and 750 ($\epsilon$ = 9220 M$^{-1}$ cm$^{-1}$) and 441 nm ($\epsilon \approx$ 6570 M$^{-1}$ cm$^{-1}$) for **2**, which are very similar to that obtained for the iron(III) complex, **3**, with the unsubstituted ligand 2-anilino-4,6-di-*tert*-butylphenol.[5c] The peak with weaker intensity at ∼440 nm accordingly can be assigned to the quinone-to-metal charge-transfer band. The high intensity suggests that allowed electronic transitions are the ligand-to-ligand $\pi-\pi^*$ charge-transfer bands, which have been also observed as dominating in earlier reported spectra for comparable complexes.[5]

**Electrochemistry.** Cyclic and square-wave voltammograms have been recorded in $CH_2Cl_2$ solutions of complexes containing 0.10 M $[TBA]PF_6$ as supporting electrolyte and a $Ag/AgNO_3$ reference electrode. Ferrocene was used as an internal standard, and the potentials are referenced versus the ferrocenium/ferrocene couple ($Fc^+/Fc$). The CV of the ferric complexes **1** and **2**, shown in Figure 1, has been recorded at fast scan rates because the reduced forms are quite labile. The CVs are essentially identical to that of complex **3** (iron complex with the unsubstituted ligand, 2-anilino-4,6-di-*tert*-butylcatechol).[5c] The oxidation potentials are +0.531 (ox2) and −0.103 (ox1) V for complex **1** and

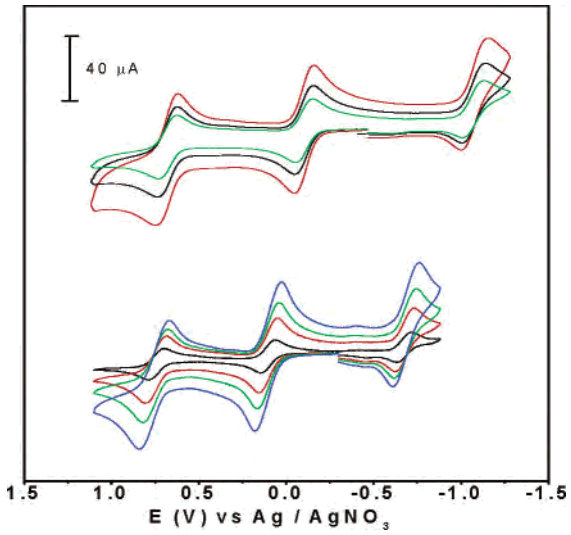


**Figure 1.** Cyclic voltammograms of complex **1** (below) at scan rates of 50, 200, 400 and 800 mV s$^{-1}$ and complex **2** (top) at scan rates of 500, 1000 and 2000 mV s$^{-1}$ at room temperature.

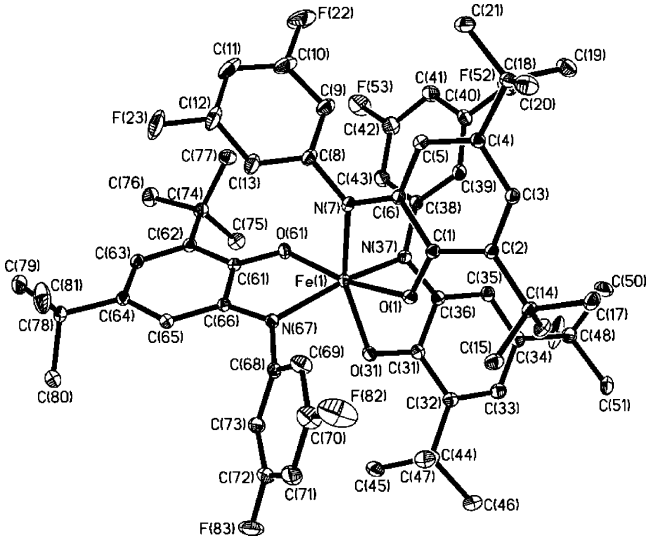


**Figure 2.** ORTEP view of $Fe(L^{F\bullet})_3$ (**1**) at 100 K with atom-numbering scheme showing 40% probability ellipsoids.

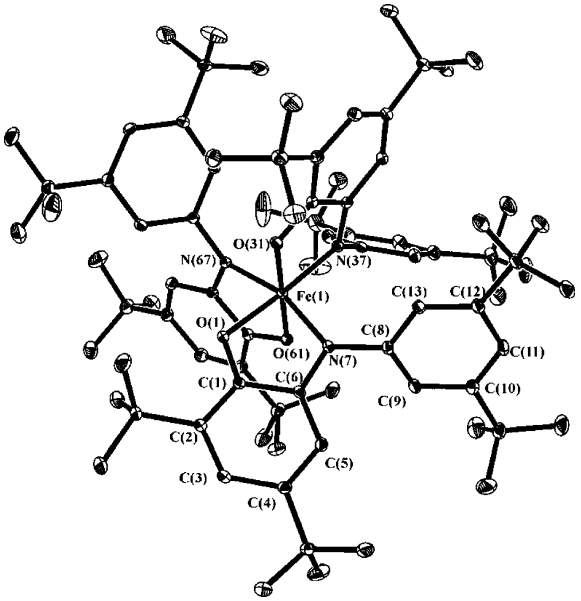


**Figure 3.** Molecular structure of the neutral complex $Fe(L^{t-Bu\bullet})_3$ (**2**) at 100 K.

+0.294 (ox2) and −0.422 (ox1) V vs $Fc^+/Fc$ for complex **2**, which can be assigned to the following redox equilibria:

$$[Fe^{III}(L^{\bullet})_3]^0 \overset{+e}{\underset{-e}{\rightleftharpoons}} [Fe^{III}(L^{\bullet})_2(L^{Q})]^{1+} \overset{+e}{\underset{-e}{\rightleftharpoons}} [Fe^{III}(L^{\bullet})(L^{Q})_2]^{2+}$$

where $L^Q$ represents the quinone form of the oxidized ligand. The reduction potentials are −0.874 for complex **1** and −1.293 V vs $Fc^+/Fc$ for complex **2**, which can be attributed to

$$[Fe^{III}(L^{\bullet})_3] \overset{+e}{\underset{-e}{\rightleftharpoons}} [Fe^{III}(L^{\bullet})_2(L^{AP})]^{-}$$

where $L^{AP}$ represents the amido-phenolate form $[L]^{2-}$ of the ligand $H_2L^R$. All these redox processes comprise a single electron transfer as evidenced by coulometric studies. Although the nature of the voltammograms is very similar, however, a shift of the waves to more positive values is observed for all three redox processes. In complex **1**, due to the strong −I effect of the fluoro group, the radical becomes less viable for oxidation to the quinone form and more viable for reduction to the amido-phenolate. A fourth and a fifth irreversible wave (not shown) at −1.268 and −1.568 V attributable to a ligand-centered and a metal-centered reduction generating the Fe(II) species, respectively, for complex **1** are also observable.

**Description of the Structures.** The crystal structures of complexes **1** and **2** have been determined by single-crystal X-ray crystallography at 100(2) K. The crystal structure of complex **2** has also been determined at 293(2) K for the reasons which are obvious from the magnetic susceptibility and Mössbauer data. Figures 2 and 3 show the structures of the neutral molecules in crystals of **1** and **2** at 100 K, respectively. Selected bond lengths and angles for complexes **1** and **2** at 100(2) and 293(2) K are summarized in Table 2 for a comparative overview.

The structures of the neutral distorted octahedral complexes **1** and **2** contain three O,N-coordinated *o*-iminobenzosemiquinonato(1−) ligands $(L^{\bullet})^-$, whose presence is clearly established by single-crystal X-ray crystallography with 2-(3,5-disubstituted anilino)-4,6-di-*tert*-butylphenol as ligands, discussed below. Complexes **1** and **2** crystallize in the monoclinic space group $C2/c$ and $P2_1/c$, respectively, whereas the corresponding Fe(III) complex **3** with the unsubstituted ligand 2-anilino-4,6-di-*tert*-butylphenol, published earlier,[5c] crystallizes in the orthorhombic chiral space group $P2_12_12_1$. The neutral molecules in these compounds possess $C_1$ symmetry and exist in two enantiomeric forms. Thus, for the compound with the unsubstituted ligand **3**, spontaneous enantiomeric resolution is observed, whereas the unit cells of **1** and **2** contain both enantiomers.

The aromatic C−C bond distances for each individual aniline phenyl group, substituted or unsubstituted, in all complexes have been found to lie within the small experimental error limits of 1.390 ± 0.01 Å, indicating that this part of the ligand is the most redox innocent one, which is not affected by the actual oxidation level of the ligand or as has been reported earlier[5] by the nature of the coordinated metal ion like $Cr^{III}$, $Mn^{IV}$, $Fe^{III}$, and $Co^{III}$. Within the small error limit, all C−C distances of these phenyl rings are equidistant in all complexes, as expected.

In contrast, the iminobenzosemiquinone part of the O,N-coordinated radicals exhibits significantly different C−C bond distances in the ring. The six C−C distances in the radical part of the ligand are not equidistant: a typical pattern of a short (av 1.374 Å), a long (av 1.429 Å), and again a short (av 1.368 Å) C−C bond and three adjacent long C−C bonds. Additionally, the average C−O and C−N bond lengths, at 1.291 ± 0.010 Å and 1.343 ± 0.013 Å, respectively, are significantly shorter than the corresponding C−O and C−N bonds of order one. Thus, this ring adopts a quinoid-type structure and yields the most significant structural parameters for the assignment of the oxidation level of a given ligand in a coordination compound. The same metrical parameters for the monoanionic radical ligands have

**Table 2.** Selected Bond Distances (Å) and Angles (deg) for **1** and **2** at 100 and 293 K

| complex **1** (100 K) | | complex **2** (100 K) | | complex **2** (293 K) | |
|---|---|---|---|---|---|
| Fe(1)−O(31) | 1.9932(8) | Fe(1)−O(31) | 1.8869(11) | Fe(1)−O(31) | 1.987(2) |
| Fe(1)−O(61) | 2.0008(8) | Fe(1)−O(61) | 1.9013(11) | Fe(1)−O(61) | 1.995(2) |
| Fe(1)−O(1) | 2.0368(8) | Fe(1)−O(1) | 1.9228(11) | Fe(1)−O(1) | 2.006(2) |
| Fe(1)−N(67) | 2.0692(9) | Fe(1)−N(67) | 1.9144(13) | Fe(1)−N(37) | 2.067(3) |
| Fe(1)−N(7) | 2.0934(10) | Fe(1)−N(7) | 1.9429(13) | Fe(1)−N(67) | 2.078(3) |
| Fe(1)−N(37) | 2.0956(9) | Fe(1)−N(37) | 1.9083(13) | Fe(1)−N(7) | 2.079(3) |
| O(1)−C(1) | 1.284(1) | O(1)−C(1) | 1.295(2) | O(1)−C(1) | 1.287(4) |
| C(1)−C(2) | 1.437(1) | C(1)−C(2) | 1.429(2) | C(1)−C(2) | 1.423(5) |
| C(1)−C(6) | 1.456(1) | C(1)−C(6) | 1.442(2) | C(1)−C(6) | 1.453(5) |
| C(2)−C(3) | 1.375(2) | C(2)−C(3) | 1.381(2) | C(2)−C(3) | 1.368(5) |
| C(3)−C(4) | 1.434(2) | C(3)−C(4) | 1.426(2) | C(3)−C(4) | 1.420(5) |
| C(4)−C(5) | 1.369(2) | C(4)−C(5) | 1.373(2) | C(4)−C(5) | 1.355(5) |
| C(5)−C(6) | 1.423(2) | C(5)−C(6) | 1.421(2) | C(5)−C(6) | 1.416(5) |
| C(6)−N(7) | 1.339(1) | C(6)−N(7) | 1.352(2) | C(6)−N(7) | 1.336(4) |
| N(7)−C(8) | 1.419(1) | N(7)−C(8) | 1.422(2) | N(7)−C(8) | 1.422(4) |
| O(31)−Fe(1)−O(61) | 108.25(3) | O(31)−Fe(1)−O(61) | 178.55(5) | O(31)−Fe(1)−O(61) | 173.53(10) |
| O(31)−Fe(1)−O(1) | 82.40(3) | O(31)−Fe(1)−N(37) | 83.42(5) | O(31)−Fe(1)−O(1) | 91.88(10) |
| O(61)−Fe(1)−O(1) | 168.92(3) | O(61)−Fe(1)−N(37) | 95.81(5) | O(61)−Fe(1)−O(1) | 93.76(10) |
| O(31)−Fe(1)−N(67) | 89.52(3) | O(31)−Fe(1)−N(67) | 95.94(5) | O(31)−Fe(1)−N(37) | 78.29(10) |
| O(61)−Fe(1)−N(67) | 77.87(3) | O(61)−Fe(1)−N(67) | 82.91(5) | O(61)−Fe(1)−N(37) | 96.04(10) |
| O(1)−Fe(1)−N(67) | 105.89(3) | N(37)−Fe(1)−N(67) | 96.29(6) | O(1)−Fe(1)−N(37) | 170.16(10) |
| O(31)−Fe(1)−N(7) | 157.74(3) | O(31)−Fe(1)−O(1) | 89.74(5) | O(31)−Fe(1)−N(67) | 99.17(10) |
| O(61)−Fe(1)−N(7) | 92.73(4) | O(61)−Fe(1)−O(1) | 91.03(5) | O(61)−Fe(1)−N(67) | 78.08(10) |
| O(1)−Fe(1)−N(7) | 76.33(3) | N(37)−Fe(1)−O(1) | 173.16(5) | O(1)−Fe(1)−N(67) | 86.04(10) |
| N(67)−Fe(1)−N(7) | 102.45(4) | N(67)−Fe(1)−O(1) | 84.54(5) | N(37)−Fe(1)−N(67) | 95.08(11) |
| O(31)−Fe(1)−N(37) | 77.38(4) | O(31)−Fe(1)−N(7) | 95.86(5) | O(31)−Fe(1)−N(7) | 97.95(10) |
| O(61)−Fe(1)−N(37) | 91.05(3) | O(61)−Fe(1)−N(7) | 85.47(5) | O(61)−Fe(1)−N(7) | 86.33(10) |
| O(1)−Fe(1)−N(37) | 88.28(3) | N(37)−Fe(1)−N(7) | 98.62(6) | O(1)−Fe(1)−N(7) | 78.01(10) |
| N(67)−Fe(1)−N(37) | 159.39(4) | N(67)−Fe(1)−N(7) | 161.92(5) | N(37)−Fe(1)−N(7) | 103.50(11) |
| N(7)−Fe(1)−N(37) | 95.31(4) | O(1)−Fe(1)−N(7) | 81.87(5) | N(67)−Fe(1)−N(7) | 156.90(10) |

**Scheme 2**

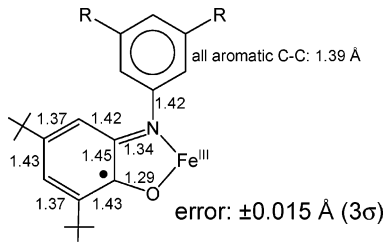


been found in the reported complexes with different metal ions [Cu(II), Ni(II), Pd(II), Cr(III), Mn(III), Mn(IV), Fe(III), and Co(III)]. It has been shown previously[5] that the aromatic ligand dianion $L^{2-}$, which is the one-electron reduced form of $(L^{\bullet})^{-}$, and the neutral one-electron oxidized quinone form $(L^{Q})^{0}$ display significantly different C−C, C−O, and C−N distances. The C−C, C−O, and C−N distances of the monoanionic radical ligand in **1** and **2** are identical within $3\sigma$ limits (±0.015 Å) and are illustrated in Scheme 2.

Interestingly, the Fe−O and Fe−N bond lengths for **1** at 100 K and for **2** at 293 K at, av 2.015 ± 0.015 Å and av 2.080 ± 0.015 Å, respectively, are in good agreement with a high-spin ferric ion description, whereas the corresponding values for **2** at 100 K are significantly shorter: Fe−O at 1.923(1), 1.887(1), and 1.901(1) Å and Fe−N at 1.943(1), 1.908(1) and 1.914(1) Å, and do not support the notion of the presence of high-spin ferric ion in **2** at 100 K.[9−11] The average iron−donor atom distances are substantially shortened upon cooling from ∼2.05 to ∼1.91 Å and strongly indicate that the spin state of the iron changes from $S = 5/2$ at 293 K to $S = 1/2$ at lower temperatures. As there is only one report[8] of spin crossover involving $S = 3/2$ in a considerably distorted six-coordinated Fe(III) system, we have not considered the $S = 3/2 \leftrightarrow S = 5/2$ transition in complex **2**; this notion is substantiated also by Mössbauer measurements.

Additionally, we note that it is not straightforward to discern among low-spin Fe(III) and low-spin Fe(II) only from the iron−donor atom distances,[9,10] thus allowing an alternative oxidation state combination for **2** at 100 K of l.s.Fe(II)$(L^{t\text{-}Bu\bullet})_2(L_{IBQ}^{t\text{-}Bu})$, in which a diamagnetic low-spin ferrous center, generated through intramolecular electron transfer, is coordinated to a neutral quinone form of the ligand $L_{IBQ}^{t\text{-}Bu}$ and two iminobenzosemiquinone radical ligands, $L^{t\text{-}Bu\bullet}$. An octahedral Ni(II) compound, $[Ni^{II}(L_{IBQ}^{CF_3})_2(OClO_3)_2]$ with two O,N-coordinated *o*-iminobenzoquinone, in which the C−O and C−N bonds of the aminophenol part of the ligand are 1.239(2) and 1.296(2) Å, has been structurally characterized;[5d] these C−O and C−N bond lengths are substantially shorter than the corresponding values in **2** (Scheme 2; Table 2), thus demonstrating the

(8) Koch, W. O.; Schünemann, V.; Gerdan, M.; Trautwein, A. X.; Krüger, H.-J. *Chem. Eur. J.* **1998**, *4*, 686−691.
(9) *Comprehensive Coordination Chemistry*; Wilkinson, G., Gillard, R. D., McCleverty, J. A., Eds.; Pergamon Press: Oxford, 1987; Vol. 4.
(10) Ross, S.; Weyhermüller, T.; Bill, E.; Bothe, E.; Flörke, U.; Wieghardt, K.; Chaudhuri, P. *Eur. J. Inorg. Chem.* **2004**, 984−997.
(11) Selected examples: (a) Juhász, G.; Hayami, S.; Sato, O.; Maeda, Y. *Chem. Phys. Lett.* **2002**, *364*, 164−170. (b) Brewer, C. T.; Brewer, G.; Jameson, G. B.; Kamaras, P.; May, L.; Rapta, M. *J. Chem. Soc., Dalton Trans.* **1995**, 37−43. (c) Conti, A. J.; Chadha, R. K.; Sena, K. M.; Rheingold, A. L.; Hendrickson, D. N. *Inorg. Chem.* **1993**, *32*, 2670−2680. (d) Kennedy, B. J.; McGrath, A. C.; Murray, K. S.; Skelton, B. W.; White, A. H. *Inorg. Chem.* **1987**, *26*, 483−495. (e) Nishida, Y.; Kino, K.; Kida, S. *J. Chem. Soc., Dalton Trans.* **1987**, 1957−1961. (f) Madea, Y.; Oshio, H.; Takashima, Y.; Mikuriya, M.; Hidaka, M. *Inorg. Chem.* **1986**, *25*, 2958−2962.

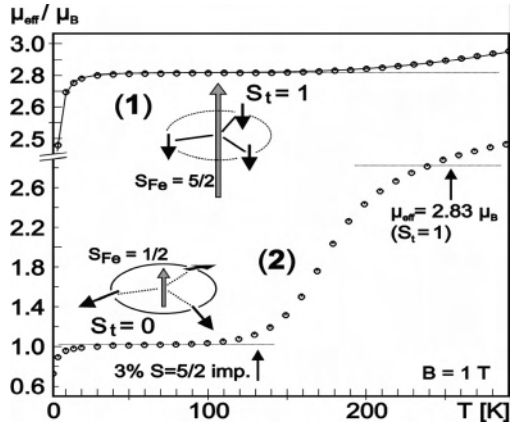


**Figure 4.** Temperature dependence of the effective magnetic moments of powder samples of complex **1** and **2**. The solid line in the trace of **1** is a spin Hamiltonian simulation described in the text. The cartoons visualize the spin coupling schemes of the low- and high-temperature forms of complex **2**.

absence of ligand oxidation level $L_{IBQ}$ in **2** and hence resulting in a physical oxidation state of +3 for iron in **2** at 100 K.

Moreover, we use the sum of the six C−C bond distances of the ring in the aminophenol derived part of the ligand to discern the oxidation states of the ligands at 100 K in **2**. The experimentally observed sum of the aminophenol ring C−C distances over all three ligands in **2** is 25.403 (0.036) Å (Table 2). By using the C−C distances for iminobenzoquinone $L_{IBQ}^{CF_3}$, as found in $[Ni(L_{IBQ}^{CF_3})_2(OClO_3)_2]$ (8.593 Å)[5d] and those for $L^{t-Bu\bullet}$ ligands in **2** (8.472, 8.464, and 8.467 Å), we can calculate the sum for a combination of two $L^{t-Bu\bullet}$ and one $L_{IBQ}$ to lie in the small range 25.524−25.532 Å. Clearly, the observed distance of 25.403 Å in **2** is shorter than the range given above, indicating strongly that the oxidation state combination for **2** at 100 K of l.s.Fe(II)$(L^{t-Bu\bullet})_2$-$(L_{IBQ}^{t-Bu})$ can be safely discarded. Thus, we conclude that complex **2** at 100 K contains three monoanionic radicals coordinated to a low-spin ferric center ($S_{Fe} = 1/2$). Magnetic susceptibility measurements, as well as Mössbauer spectroscopy, were performed on **1** and **2** at different temperatures to shed more light on this problem.

**Magnetic Susceptibility Measurements.** To establish the electronic structures for complexes **1** and **2**, variable-temperature (2−290 K) magnetic susceptibility measurements were performed on powdered samples of **1** and **2** by using a SQUID magnetometer with $B = 1.0$ T applied field.

Figure 4 (top) shows the temperature dependence of the effective magnetic moment, $\mu_{eff}(T)$, for complex **1**. In the range 30−200 K, nearly temperature-independent values of 2.80−2.84 $\mu_B$ are observed, which correspond to the spin-only value for $S = 1$ (2.828 $\mu_B$). Above 200 K, the effective moment increases slowly and reaches a value of 2.95 $\mu_B$ at 290 K. This indicates the onset of thermal population of excited spin manifolds. Below 30 K, $\mu_{eff}(T)$ falls off, as expected on account of field saturation and zero-field splitting (zfs) of the ground state.

The $S_t = 1$ ground state of complex **1** can result only from antiparallel spin alignment of the central high-spin ferric ion ($S_{Fe} = 5/2$) and the three iminosemiquinone ligand radicals ($S_R = 1/2$, see cartoon in Figure 4, top). Apparently, other states with higher total spins, as they arise from the competing interactions between iron and three radicals, are less favorable and appear at higher energies. Thus, strong antiferromagnetic (a.f.) exchange coupling exists between the high-spin iron center and the ligand radicals and stabilizes the triplet ground state against putative a.f. radical−radical interaction. The same situation was encountered for complex **3** with the unsubstituted ligand.[5c]

**Chart 1.** Spin Coupling Scheme and Energy Distribution for the a.f. Interaction of Low-Spin Iron(III), $S_{Fe} = 1/2$, and Three Ligand Radicals, $S_R = 1/2$, with Spin Frustration Due to $C_3$ Symmetry[a]

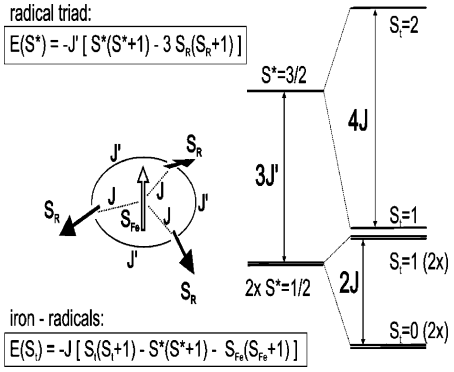


[a] The equations hold also for the high-spin model with $S_{Fe} = 5/2$.

The energy gap between the ground state of **1** and the excited states can be estimated from the rise of $\mu_{eff}(T)$ above 200 K. To this end, the magnetic data of **1** were simulated by using the Hamiltonian

$$H = H_{ex} + D_{Fe}[S_{Fe,z}^2 - 35/12] + \sum_{i=1,3,Fe} g_i \mu_B S_i B \qquad (1)$$

where

$$H_{ex} = -2J \sum_{i=1,3} S_{Fe} S_i - 2J' \sum_{i \neq j=1,3} S_i S_j \qquad (2)$$

For the sake of simplicity, eq 2 is based on the assumption of $C_3$ symmetry for the spin topology of **1**, in which the radicals form a symmetric spin triad that is symmetrically coupled to the central *S*-state ferric ion. $J$ and $J'$ represent the coupling constants for the isotropic iron−radical and radical−radical exchange interactions, and the other parameters have their usual meaning. (The symmetry approximation is not quite correct since the iron is not on a cubic site, as can be seen from the presence of quadrupole splitting in the Mössbauer spectra of **1**, but slightly broken symmetry would induce only minor modifications of the results.)

If level mixing by zero-field splitting (zfs) or other anisotropies are neglected, eq 2 yields eight spin manifolds, which in terms of the total spin are one triplet ($S_t = 1$), three quintets ($S_t = 2$), three septet ($S_t = 3$), and one nonet ($S_t = 4$). For dominating, strong a.f. $J$ coupling, the triplet is ground state and the first excited states are the three quintets at energies $\Delta_1 = -4J$ and $\Delta_{2,3} = -7J + 3J'$ (these energies are derived from the equations given in Chart 1, top and bottom). It is remarkable that the first excited state does not depend on $J'$ for any $|J| \geq |J'|$, and on the other hand, the triplet remains the ground state for any $|J'| < 7/3\ |J|$. This

means, that a.f. *radical−radical* coupling would have to be very strong to alter the total spin ground state in this system.

A fit of the experimental data for complex **1** by using eqs 1 and 2 yields an excellent simulation with $J = -184(5)$ $cm^{-1}$ and $J'$ set to zero, and the other variables being $g_{Fe} = 2.00(3)$, $g_i = 2.0$ fixed, and $D_{Fe} = 3.1(3)$ $cm^{-1}$ (Figure 4, top, solid line). According to the expressions for $\Delta_1$ and $\Delta_2$, the value of $|J|$ represents a lower limit for the strength of the a.f. exchange interaction between iron(III) and the radicals, but $J'$ may be of the same strength or even larger (for comparison: for $J' = J$ where the three quintets are degenerate, the fit value is $-230$ $cm^{-1}$).

Figure 4 (bottom) displays the magnetic data of a powdered sample of complex **2** in the range from 2 to 290 K. At low temperatures up to 120 K, only an unusual weak effective moment $\mu_{eff}$ of about 1 $\mu_B$ is measured which shows the normal fall off below 10 K to base temperature. This weak paramagnetic moment, which is distinctly below the spin only value for $S = 1/2$ ($\mu_{eff}^{s.o.} = 1.73\,\mu_B$), was persistent in several different preparations of **2**, even with repeated recrystallization protocol. Nevertheless, it is a paramagnetic impurity (3% of $S = 5/2$), as comes out from applied-field Mössbauer spectra shown below. The spectra recorded in this temperature regime unambiguously disclose the molecular spin state $S_t = 0$ for **2** from the absence of internal fields at the Mössbauer nucleus. The result discards alternative interpretations of the weak paramagnetism of the samples of **2**, like the presence of a permanent high-spin contribution from incomplete spin transition (which would correspond to 13% $S = 1$ species).

Above 130 K, $\mu_{eff}(T)$ of complex **2** increases rapidly and reaches the spin-only value for $S = 1$ (2.873 $\mu_B$) at about 250 K, but the curve levels off only beyond the detection limit of 290 K with 3.04 $\mu_B$ ($\chi_M T = 1.1589$ $cm^3$ K $mol^{-1}$). The sigmoid appearance of the temperature curve with an inflection point at about 175 K suggests the presence of a phase transition in the solid material. This is in accordance with the spin crossover, as it is inferred earlier for the central ferric ion of **2** from the high- and low-temperature X-ray diffraction data. The temperature variations of the magnetic data are fully reversible, and the samples do not show any indication of thermal hysteresis upon temperature cycling (not shown). Such gradual spin transitions without thermal hysteresis are known for iron(III) complexes and were reported earlier.[6,11] We note that, in this particular case of complex **2** with four interacting spins, the true transition temperature cannot be readily obtained from magnetic susceptibility data, since spin transition and thermal population of excited states in the high-temperature fraction occur simultaneously, which obscures the interpretation of individual processes.

**Zero-Field Mössbauer Spectra.** The 80 K Mössbauer spectrum of solid complex $Fe(L^{F\bullet})_3$ (**1**) as shown in Figure 5A corroborates the iron high-spin $3d(t_{2g})^3(e_g)^2$ configuration introduced above. The isomer shift, $\delta = 0.54$ mm $s^{-1}$, and quadrupole splitting, $|\Delta E_Q| = 0.88$ mm $s^{-1}$, are typical for octahedral high-spin ferric species.

**Valence States of Compound 2.** We have recorded Mössbauer spectra of solid complex $Fe(L^{t-Bu\,\bullet})_3$ (**2**) in the temperature range 4.2−297 K to elucidate the spin transition and coupling schemes. The Mössbauer parameters are listed in Table 3, and a selection of zero-field spectra is depicted in Figure 5B. The spectra change gradually with temperature from small isomer shift and large quadrupole splitting in the range 4.2−160 K to distinctly larger isomer shift and smaller quadrupole splitting above 250 K. The variation reflects the spin crossover seen in the magnetic data and the molecular structure of **2**. While the variation of the isomer shift is strictly monotonic in this process, the quadrupole splitting virtually collapses at the transition point around 200 K and increases again at 250−295 K. The lowest value measured was 0.22 mm $s^{-1}$. At neither temperature is a superposition of resolved subspectra from high- and low-temperature states observed, nor any indication of line broadening. This reveals a fast spin crossover mechanism with fluctuation rates of the electronic structure exceeding the lifetime of the $^{57}Fe$ nucleus and the nuclear quadrupole precession time ($\tau_{relax} \ll 10^{-7}$ s). The slight asymmetry in the relative line intensities of the spectra can be readily assigned to nonperfect sample preparation with partially aligned powder distribution (texture). The change of the asymmetry during the transition form high- to low-temperature phase was even a first indication of different signs of the electric field gradient tensor (efg) in these regimes (see below).

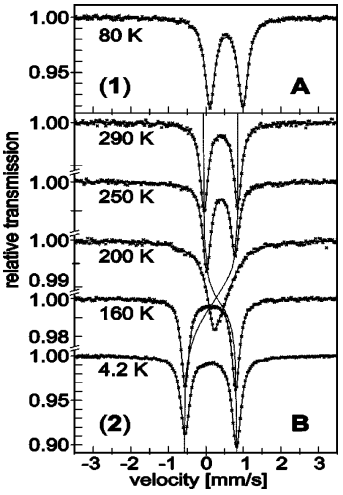


**Figure 5.** Zero-field Mössbauer spectra of solid complex **1** (A) and complex **2** (B) at different temperatures. The thin dotted lines are artistic guide lines to indicate the variation of the Mössbauer lines through the spin crossover of **2**.

**Table 3.** Mössbauer Isomer Shift and Quadrupole Splitting Parameters of Solid **2**

| $T$ [K] | $\delta$ [mm $s^{-1}$] | $\Delta E_Q$ [mm $s^{-1}$][a] | $\eta$[b] |
|---|---|---|---|
| 4.2 | 0.13 | −1.37 | 0.43 |
| 80 | 0.13 | −1.37 | |
| 120 | 0.14 | −1.37 | |
| 140 | 0.12 | −1.35 | 0.45 |
| 160 | 0.12 | −1.34 | |
| 200 | 0.31 | (−)0.22 | |
| 240 | 0.38 | +0.75 | 0.32 |
| 250 | 0.40 | +0.76 | |
| 290 | 0.40 | +0.89 | |
| 297 | 0.39 | +0.92 | |

[a] Signs are inferred from applied measurements at 4.2, 140, and 240 K. [b] The asymmetry parameter of the electric field gradient tensor $V_{ij}$: $\eta = (V_{xx} - V_{yy})/V_{zz}$.

The Mössbauer isomer shift of **2** in the low-temperature regime up to about 120 K is remarkably low ($\delta = 0.13$ mm $s^{-1}$), whereas the quadrupole splitting is quite large for a quasi-octahedral compound ($|\Delta E_Q| = 1.37-1.34$ mm $s^{-1}$). Together, both parameters strongly indicate the presence of low-spin iron(III) with $3d(t_{2g})^5$ configuration and $S_{Fe} = 1/2$. Very similar Mössbauer parameters are found, for instance, for the typical ferric low-spin complexes of the type $[Fe(phen)_3](ClO_4)_3$ which have six 'hard' donor ligands similar to compound **2** ($\delta = 0.10$ mm $s^{-1}$, $|\Delta E_Q| = 1.71$ mm $s^{-1}$ at 80 K).[13]

For an obvious interpretation of the diamagnetic ground state of compound **2**, one might be tempted to consider alternatively the presence of ferric *intermediate* spin with $S_{Fe} = 3/2$ (and a.f. coupling with three ligand radicals). However, this option can be clearly ruled out, since significantly larger and *positive* quadrupole splitting would be expected ($\Delta E_Q(80\ K) \geq +2.3 - +3$ mm $s^{-1}$),[14] in contrast to the *negative* quadrupole splitting measured for **2**. (For the determination of the sign of $\Delta E_Q$, see magnetic Mössbauer spectra below.) Moreover, the ferric low-spin state is in accordance with the presence of the six similar strong, quasi-octahedral ligands in **2**, whereas the $3d^5$ intermediate-spin configuration is usually related to another orbital scheme with one *single* d orbital being highly destabilized above the other four due to an exceedingly stronger axial distortion of the ligand field. Typically, this situation is achieved with penta-coordination and weak apical ligands.[14] At least all of the reported intermediate-spin ferric complexes are five-coordinated except one with strongly distorted 6-fold coordination.[8]

We also note that another alternative valence state of the iron can be specifically discarded from the Mössbauer data, namely the presence of low-spin Fe(II) with $S_{Fe} = 0$. This option would imply internal electron transfer and the presence of a doubly oxidized nonradical ligand, so that only two ligand radicals would be left. These could easily yield the $S_t = 0$ ground state by means of a.f. coupling. However, in contrast to the Mössbauer data of **2**, the $3d(t_{2g})^6$ configuration of six-coordinate low-spin Fe(II) with quasi-octahedral ligand field symmetry typically exhibits small quadrupole splittings according to the vanishing valence contribution to the electric field gradient tensor.[12] Moreover, the isomer shifts are larger and found in the range $0.35-0.55$ mm $s^{-1}$. The archetypical examples are ferrous phenanthroline complexes $[Fe(phen)_2](X)_2$ where X may be $(ClO_4)$, NCS, or $(NO_2)$.[15] These show values at liquid nitrogen temperatures of $\delta = 0.34-0.44$ mm $s^{-1}$ and $\Delta E_Q = 0.23-0.53$ mm $s^{-1}$. Similar values are found for ferrous porphyrin or other macrocyclic complexes.[16] The Mössbauer result corroborates the conclusion from the interpretation of the molecular structure from above where a ligand oxidation (and intramolecular iron reduction) could be excluded.

In the high-temperature regime above 250 K, the Mössbauer parameters of **2** closely resemble those of complex **1** ($\delta(290\ K) = 0.40(1)$ mm $s^{-1}$, $\Delta E_Q = 0.9$ mm $s^{-1}$), which indicates high-spin state $S_{Fe} = 5/2$. The slightly lower isomer shift of **2** at 290 K than that of **1** at 80 K is mostly due to different second-order Doppler shift at this temperature, but also some minor fraction of the low-spin state may still be present. In summary, the Mössbauer spectra substantiate the presence of a typical high-spin ↔ low-spin equilibrium for the ferric iron of compound **2**.

**Temperature Dependence of Compound 2.** The peculiar drop of the Mössbauer quadrupole splitting at the transition temperature of the spin crossover of **2** can be explained by a dynamic averaging of two collinear electric-field gradient (efg) tensors with opposite main components for the low- and high-spin configuration. Fast fluctuations of the electronic structure between the two configurations averages the efg experienced by the $^{57}Fe$ nucleus for each molecule. As a consequence, the Mössbauer quadrupole lines are relaxing crosswise, i.e., the low-energy Mössbauer line of the low-spin quadrupole doublet and the high-energy line of high-spin doublet show a common coalescence pattern, and vice versa. The weight factors for the two efg components are temperature dependent, as given by the spin equilibrium. As a result, the Mössbauer lines shift toward each other and crossover at the transition temperature where the low- and high-spin fractions are equal. This is indicated by dotted guide lines shown in Figure 5.

A quantitative deconvolution of the experimental Mössbauer quadrupole splittings by using this model yields independent information about the high-spin ↔ low-spin transition curve without being obscured by superimposed changes in the spin state population, as it is encountered for the interpretation of the magnetization data. The temperature-dependent average of two collinear efg tenors could nicely reproduce the experimental values of $\Delta E_Q(T)$ with values for the relative fraction of high-spin state as indicated by the symbols (◇) given in Figure 6. The dashed line through these points is just an artistic guide for the eye to indicate the true transition curve. The main component and the asymmetry parameter of the efg for the low-spin fraction were readily taken from the magnetic Mössbauer spectra at 4.2 K as shown below, whereas the efg of the high-spin fraction was determined from the fit to the experimental quadrupole splittings. In this procedure, we neglected any small intrinsic temperature variations of the pure high- and

(12) Gütlich, P.; Link, R.; Trautwein, A. X. *Mössbauer Spectroscopy and Transition Metal Chemistry*; Springer-Verlag: Berlin, 1978.
(13) Berrett, R. R.; Fitzsimmons, B. W.; Owusu, A. *J. Chem. Soc. A* **1968**, 1575−1579.
(14) (a) Maltempo, M. M.; Moss, T. H. *Quart. Rev. Biophys.* **1976**, *9*, 181−215. (b) Maltempo, M. M. *J. Chem. Phys.* **1974**, *61*, 2540−2547. (c) Ganguli, P.; Marathe, V. R.; Mitra, S. *Inorg. Chem.* **1975**, *14*, 970−973. (d) Niarchos, D.; Kostikas, A.; Simopoulos, A.; Coucouvanis, D.; Piltingsrud, D.; Coffman, R. E. *J. Chem. Phys.* **1978**, *69*, 4411−4418. (e) Wickman, H. H.; Trozzolo, A. M. *Inorg. Chem.* **1968**, *7*, 63−68. (f) Kostka, K. L.; Fox, B. G.; Hendrich, M. P.; Collins, T. J.; Rickard, C. E. F.; Wright, L. J.; Münck, E. *J. Am. Chem. Soc.* **1993**, *115*, 6746−6757. (g) Keutel, H.; Käpplinger, I.; Jäger, E.-G.; Grodzicki, M.; Schünemann, V.; Trautwein, A. X. *Inorg. Chem.* **1999**, *38*, 2320−2327. (h) Evans, D. R.; Reed, C. A. *J. Am. Chem. Soc.* **2000**, *122*, 4660−4667. (i) Ghosh, P.; Bill, E.; Weyhermüller, T.; Wieghardt, K. *J. Am. Chem. Soc.* **2003**, *125*, 3967−3979.
(15) Long, G. In *Mössbauer Spectroscopy*; Dickson, D. P. E., Berry, F. J., Eds.; Cambridge University Press: Cambridge, 1986; pp 70−142.
(16) (a) Debrunner, P. G. In *Iron Porphyrins Part III*; Lever, A. B. P., Gray, H. B., Eds.; VCH: Weinheim, 1989; Vol. III, pp 137−234. (b) Meyer, K.; Bill, E.; Mienert, B.; Weyhermüller, T.; Wieghardt, K. *J. Am. Chem. Soc.* **1999**, *121*, 4859−4876.

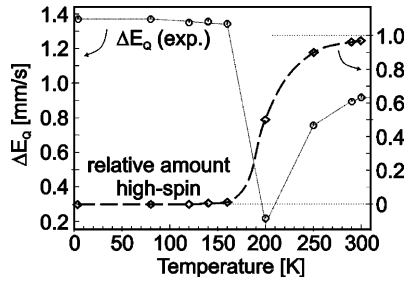


**Figure 6.** Temperature dependence of the Mössbauer quadrupole splitting of complex **2** (symbols ○) and the relative fraction of ferric high-spin state (symbols ◇) obtained from the model of averaged efg tensors. The dashed line is an artistic guide lines to indicate the spin crossover transition. The efg parameters for the pure low-spin and high-spin components were $\Delta E_{Q,LS} = -1.37$ mm s$^{-1}$, $\eta_{LS} = 0.43$ and $\Delta E_{Q,HS} = +1.1$ mm s$^{-1}$, $\eta_{HS} = 0.2$.

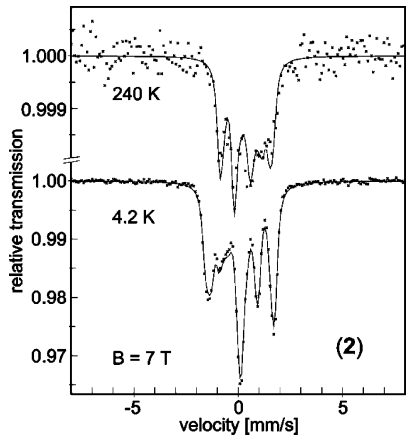


**Figure 7.** Applied-field Mössbauer spectra of solid complex **2** recorded at 4.2 and 240 K with 7 T field applied perpendicular to the $\gamma$ beam. The solid lines are spin Hamiltonian simulations.

low-spin efg's. (A deconvolution of the isomer shifts would be certainly much more affected by such an approximation due to second-order Doppler shift, particularly in the high-temperature branch.) We note that the apparent inflection point at about 200 K in the transition curve obtained from the Mössbauer quadrupole splittings is a bit higher than the transition temperature of 175 K suggested by the magnetic data.

**Magnetic Mössbauer Spectra of Compound 2.** The assumption of different signs for the main components of the efg tensors in high-spin and low-spin states of **2** could be readily corroborated from the applied-field spectra recorded at 4.2 K and 240 K ($B_{\perp\gamma} = 7$ T) shown in Figure 7. The efg parameters at 4.2 K are found to be $\Delta E_Q = -1.37$ mm s$^{-1}$ and $\eta = 0.4(1)$, whereas the 240 K spectrum reveals $\Delta E_Q = +0.76$ mm s$^{-1}$ and $\eta = 0.3(1)$. Note that in Figure 6 at 240 K there is still about 35% of the low-spin fraction present (for technical reasons, we did not measure applied-field spectra at higher temperatures). Since both efg tensor parameters, $\Delta E_Q$ and $\eta$, are in perfect agreement with the deconvolution model ($\Delta E_{Q,HS} = +1.1$ mm s$^{-1}$, $\eta_{HS} = 0.2$), also the approximation of collinear high- and low-spin efg tensors should be reasonable.

Moreover, the 7 T spectrum of **2** at 4.2 K can be perfectly simulated with the applied field only. This excludes paramagnetism and reveals a purely diamagnetic ground state ($S_t = 0$) of the compound. At 240 K, the simulation was performed with the simplifying assumption of an $S_t = 1$ total spin state to account for the paramagnetic behavior in the high-spin state of **2**. With the zfs parameter $D$ and $E/D$ being fixed to 3 cm$^{-1}$ and zero, the best fit was obtained (in the limit of fast-spin relaxation) with $A$-tensor components $A_t/g_N\beta_N = (-20.8, -20.8, -29.3)$ T to account for the presence of weak internal fields at the Mössbauer nucleus. The values would be close to what is expected for high-spin Fe(III), but we cannot really convert it to the local $A$-tensor components since the true coupling scheme of the four-spin system is not known from the few data. In summary, the magnetic Mössbauer spectra prove diamagnetism of **2** at low temperature and reveal the full efg tensor with opposite signs of the main components in low- and high-spin states of the molecule.

**Spin Coupling in Compound 2.** The most intuitive rationalization of the diamagnetic ground state of complex **2** at low temperature could probably be based on the ad-hoc assumption of antiferromagnetic coupling between an intermediate-spin ferric ion with $S_{Fe} = 3/2$ and three ligand radicals ($3 \times S_R = 1/2$). The observed spin crossover would then be an unusual, however not unprecedented, $3/2 \leftrightarrow 5/2$ transition.[17] This possibility, however, is refuted by the Mössbauer data, which clearly favor ferric low-spin configuration for the metal ion of **2** ($S_{Fe} = 1/2$). The Mössbauer result, like the structural data of compound **2**, rules out also the other intuitive possibility, which is the presence of an intrinsic electron transfer state with a low-spin iron(II) ($S_{Fe} = 0$), a quinone and two a.f. coupled radical ligands ($2 \times S_R = 1/2$).

Thus, the spin transition of solid complex **2** results from an $S = 1/2 \leftrightarrow S = 5/2$ spin crossover of the ferric ion and the singlet ground state ($S_t = 0$) observed at low-temperatures arises from competing antiferromagnetic interactions of the low-spin iron center ($S_{Fe} = 1/2$, $t_{2g}^5$) and the three equivalent $\pi$ radicals ($3 \times S_R = 1/2$). Apparently, super-exchange interaction between the ligand radicals plays a crucial role in this scheme, since the iron−radical coupling alone cannot stabilize a diamagnetic state. The magnetic properties of **2** are best described if the three ligand radicals are treated first as an a.f. coupled triad of $3 \times S_i = 1/2$, which exhibits a quartet and two doublets with 'local' subspins $S^* = 3/2$ and $2 \times S^* = 1/2$. One (or both) of the doublets are the 'local' ground state of the triad, which then is a.f. coupled to iron ($S_{Fe} = 1/2$) yielding the total spin $S_t = 0$ ground state. The approach is most intuitive if the a.f. radical−radical interaction is stronger than the iron−radical coupling, but it is generally valid for construction of the whole set of total spin states.

In the following, we will again adopt $C_3$ symmetry for the spin topology of **2**, similar to what we did above for compound **1**. Equation 2 is applied for description of the spin coupling with two coupling constants, $J$ and $J'$, for the individual iron−radical and radical−radical exchange interactions, respectively. One might argue that here the $3d(t_{2g})^5$ configuration of low-spin iron(III) does not justify such a

(17) Chun, H.; Weyhermüller, T.; Bill, E.; Wieghardt, K. *Angew. Chem., Int. Ed.* **2001**, *40*, 2489−2492.

simplification, since the iron spin should be virtually located in a single (octahedral) d orbital. However, the point symmetry at the iron site is only $C_1$ and the basic d orbitals must be mixed by low-symmetry elements (and spin−orbit coupling). In fact, this seems to be corroborated by the moderately small Mössbauer quadrupole splitting for a ferric low-spin compound, which indicates small valence contribution to the efg according to a distribution of the hole in the '$t_{2g}$ shell'. Moreover, the radical ligands are twisted against any basic octahedral coordinate system, so that the overlap of none of the (fairly delocalized) ligand magnetic orbitals with any iron magnetic orbital and none of the superexchange pathways between the ligands appears to be clearly favored. Therefore, a symmetrized spin topology seems to be a reasonable starting point. Low-symmetry differences in the individual coupling strengths can affect the exact energy separations and lift all degeneracy present for symmetric triad, but basic picture will not be changed.

The suggested spin-coupling scheme for the ground state of compound **2** is visualized by the cartoon at the bottom of Figure 4; further details are given in Chart 1. In the symmetric model, the ground state of the radical triad is degenerate (so-called 'spin-frustration'). The energies $E(S^*,S_t)$ of the total spin states $(S^*,S_t)$ can be generally given as $2 \times E(1/2,0) = +3/2J$; $2 \times E(1/2,1) = -1/2J$; $E(3/2,1) = -3J' + 5/2J$; $E(3/2,2) = -3J' - 3/2J$ (energy zero set to doublets $S^* = 1/2$). The example presented in Chart 1 sketches a situation where the radical−radical and iron-radical coupling constants $J'$ and $J$ have about the same value. From the energy relations, it is clear that the prevailing ground state is a singlet already for $|J'| > 1/3\ |J|$ (in some contrast to first intuition!).

The plateau in the experimental magnetic moment of **2** extends up to about 100 K (Figure 4, bottom), whereas the Mössbauer quadrupole splittings indicate pure low-spin state of the ferric ion up to about 160 K. This shows onset of thermal population of the excited triplet(s) at about 100 K. The rise in $\mu_{eff}(T)$ can be simulated by using eqs 1 and 2 in order to obtain a lower limit for the energy of the excited spin state. In the symmetric model with $J' = J$ (the three triplets at same energy), a value for the energy gap $\Delta = |2J|$ of 460 $cm^{-1}$ is obtained (not shown). This again can only represent an estimate of the lower limit for the iron−radical exchange coupling constant.

The paramagnetic high-temperature phase of complex **2** for which the metal ion is ferric high-spin, presumably exhibits an $S_t = 1$ intrinsic electronic ground state like complex **1**. Since the Mössbauer analyis clearly renders the iron high-spin in this state, it is obvious to assume that dominating *iron−radical* coupling achieves antiparallel spin alignment $S_{Fe} = 5/2$ and the three ligand radicals, $S_R = 1/2$, like for **1**. Even the rise of $\mu_{eff}(T)$ above 200 K to values beyond those of a triplet (Figure 4, lower trace) resembles that observed for complex **1**. In summary, compelling similarity can be stated for compound **1** and the high-spin form of **2**.

**Concluding Remarks.** To conclude, the following points of this study deserve particular attention.

Two noninnocent ligands, 2-(3,5-difluoroanilino)-4,6-di-*tert*-butylphenol, $H_2L^F$, and 2-(3,5-di-*tert*-butylanilino)-4,6-di*tert*butylphenol, $H_2L^{t-Bu}$, have been used to synthesize two new radical-containing Fe(III) compounds. As expected, complex **1**, $Fe(L^{F\bullet})_3$, exhibits strong antiferromagnetic coupling operating between three radicals ($S_R = 1/2$) and the high-spin Fe(III) center ($S_{Fe} = 5/2$) yielding an $S_t = 1$ as the ground state. In contrast, complex **2** $Fe(L^{t-Bu\bullet})_3$, contains a low-spin Fe(III) ($S_{Fe} = 1/2$) and three *o*-iminosemiquinone radicals ($S_R = 1/2$), resulting in a diamagnetic ground state below ~100 K. The singlet ground state ($S_t = 0$) owes its origin to the condition $|J'| > 1/3\ |J|$, where $J'$ represents the radical−radical coupling and $J$ the antiferromagnetic iron−radical coupling. The Mössbauer data rules out the other intuitive rationalizations. The sigmoidal appearance of the magnetic data indicates the spin crossover phenomenon of the central ferric ion. *No other bidentate N,O-chelating donor set is known to impart spin-transition property until now in any ferric complex.*

The nature of the meta substituents at the aniline moieties causes a change in the strength of the ligand field imparted to the ferric centers of complexes **1** and **2** in the expected manner: electron-withdrawing groups decrease the electron density on the N atom of the aniline moiety whereas electron-pushing groups act oppositely; thus, the ligand with the *tert*-butyl substituents causes spin-pairing resulting in a low-spin Fe(III) in complex **2**. Noteworthy is that the transfer of the polar properties of the ortho and para substituents (I effect) through the benzene ring is facilitated by the $\pi$ delocalization in the ring. Hence, the observed effect of the meta substituents on the ligating property of $H_2L^R$ owes most probably its origin to the $\sigma$ framework of the ligands. This rationalization is in accord with the ground-state $S_t = 1$ for complex **3**, $Fe(L^{H^c})_3$, containing a high-spin Fe(III) ($S_{Fe} = 5/2$) and three radicals ($3 \times S_R = 1/2$) reported earlier by us.[5c]

Electrochemical measurements indicate redox processes, which are mainly ligand-centered. Thus, for each complex, a number of oxidations and reductions, resulting in quinoid and phenolate forms of the ligands, respectively, are discernible. The nature of the substituents on the aniline moiety of the ligand causes a shift of the reversible redox potentials in the expected manner, i.e., electron-withdrawing groups facilitate the reductions and impede the oxidations and vice versa.

**Acknowledgment.** Financial support from the German Research Council (DFG) is gratefully acknowledged (Project: Priority Program Ch111/2-2). Skillful technical assistance of Mrs. H. Schucht, Mrs. R. Wagner, Mr. A. Goebels, Mr. Mienert, and Mr. U. Pieper is thankfully acknowledged.

**Supporting Information Available:** Crystallographic data in cif format. This material is available free of charge via the Internet at http://pubs.acs.org.

IC050885L